

# Energy Dependent Time Delays of kHz Oscillations due to Thermal Comptonization

Nagendra Kumar<sup>1\*</sup> and Ranjeev Misra<sup>1</sup>

<sup>1</sup>*Inter-University Centre For Astronomy and Astrophysics, Post Bag4, Ganeshkind, Pune-411007, India*

## ABSTRACT

We study the energy dependent photon variability from a thermal Comptonizing plasma that is oscillating at kHz frequencies. In particular, we solve the linearised time dependent Kompaneets equation and consider the oscillatory perturbation to be either in the soft photon source or in the heating rate of the plasma. For each case, we self consistently consider the energy balance of the plasma and the soft photon source. The model incorporates the possibility of a fraction of the Comptonized photons impinging back into the soft photon source. We find that when the oscillation is due to the soft photon source, the variation of the fractional root mean square (r.m.s) is nearly constant with energy and the time-lags are hard. However, for the case when the oscillation is due to variation in the heating rate of the corona, and when a significant fraction of the photons impinge back into the soft photon source, the r.m.s increases with energy and the time lags are soft. As an example, we compare the results with the  $\sim 850$  Hz oscillation observed on March 3, 1996 for 4U 1608-52 and show that both the observed soft time-lags as well as the r.m.s versus energy can be well described by such a model where the size of the Comptonizing plasma is  $\sim 1$  km. Thus, modelling of the time lags as due to Comptonization delays, can provide tight constraints on the size and geometry of the system. Detailed analysis would require well constrained spectral parameters.

**Key words:** stars: neutron – X-rays: binaries – X-rays: individual: 4U 1608–52 – radiation mechanisms: thermal

## 1 INTRODUCTION

X-ray binaries harbour compact objects and their X-ray luminosity is believed to be generated due to an accretion disk formed by material accreted from a companion star. The X-ray emission is known to vary on a wide range of timescales. It was after the launch of the *Rossi X-ray Timing Explorer* (RXTE) satellite, that millisecond variability was detected in several sources (for reviews see for e.g. van der Klis 2000, 2006; Remillard, & McClintock 2006). The X-ray variability is typically quantified in the frequency domain by computing the power density spectra. The power density spectrum sometimes shows peaked features which are termed as quasi-periodic oscillations (QPO). In some neutron star low-mass X-ray binaries (LMXBs), there are QPOs observed in the frequency range of 400 to 1300 Hz, and these are termed as kilohertz QPOs. Often two simultaneous kHz QPOs are observed in a system, with the higher-frequency one being called the ‘upper kHz QPO’ while the lower-frequency one is called the ‘lower kHz QPO’. In general, the quality factor,  $Q$ , which is the ratio of the QPO frequency to the full width at

half maximum, of the lower kHz QPO is significantly greater than the upper one (Mendez 2006).

There have been several models invoked to explain this twin kHz QPO phenomena. A list of different models with their merits and demerits has been presented by Lin, et.al. (2011). Here we briefly mention some of them. In the sonic-point model (Miller, Lamb, & Psaltis 1998; Lamb, Miller, & Psaltis 1998) with modifications (Lamb, & Miller 2003), the frequency of the upper kHz QPO is interpreted as the Keplerian one at the sonic radius, while the frequency of lower kHz QPO is generated by the modulation of the upper QPO with the neutron star spin frequency. In this interpretation, the frequency separation between the upper and lower kHz QPO should be a constant, but almost all sources show significant variation in the separation. For example, for the LMXB 4U 1608-52 a linear relation between the upper and lower kHz QPO has been reported (Mendez, et.al. 1998; Belloni, Mendez, & Homan 2005, 2007). The relativistic precession model (Stella, & Vietri 1999) identifies the upper kHz QPO frequency as a Keplerian one with the lower kHz QPO generated due to modulation of the Keplerian frequency with the relativistic periastron precession frequency. In the two-oscillator model (Osherovich, & Titarchuk 1999;

\* E-mail:nagendrak@iucaa.ernet.in

Titarchuk, Osherovich, & Kuznestov 1999), the lower kHz QPO is due to a blob moving in a Keplerian orbit, and the upper kHz QPO is generated by the influence of the Coriolis force on the blob when it enters the neutron star's rotating magnetosphere. Later, Titarchuk (2003) refined this model by connecting the QPO to a Rayleigh-Taylor gravity wave. Fragile, Mathews, & Wilson (2001) have proposed that the accretion disk around a rapidly rotating compact object may be misaligned beyond a transition radius due to the Bardeen-Petterson effect and this gives rise to the QPO phenomenon.

There have also been attempts to understand these QPOs as global oscillation in the disk due to hydrodynamic or magneto-hydrodynamic (MHD) instabilities or waves. In a series of papers, Kato (e.g. 2007, 2009) the QPO is explained to be generated by a resonant excitation caused by the non-linear interactions between the disk oscillation modes. The phenomena has been attributed to Alfvén wave oscillations (Zhang 2004) or to standing modes of MHD waves (Li, & Zhang 2005). The Rossby wave instability in the inner disk has also been invoked (Lovelace, Turner, & Romanova 2009; Lovelace, & Romanova 2007). Shi, & Li (2009) have tried to explain the QPOs in terms of a resonant coupling of MHD oscillation modes with the neutron star spin. Bachetti, et.al. (2010) have performed MHD simulations to understand the phenomena.

Apart from theoretical consistencies, the validity of these different models can in principle be tested with observations. A model should explain the observed relationships between the twin kHz QPO frequencies and any other lower frequency QPOs (e.g. Straaten, van der Klis, & Mendez 2003; Altamirano, et.al. 2008). It may also need to explain the strength of the kHz QPOs (e.g. Barret, Olive, & Miller 2005; Mendez 2006) or the condition for the appearance of two kHz QPOs (e.g. Sanna, et. al. 2012; Mendez 2006; Lin, et.al. 2012; Mendez, et.al. 1998). Unfortunately, there is no consensus that any of the models is the most favourable one. This is primarily because none of the models have a clear predictive and distinguishing signature which can be tested against these observations.

It is also not clear how does a dynamical oscillation proposed by these different models, couples to the radiative process that produces the X-ray emission. Relatively fewer studies have been undertaken to identify the radiative mechanism that is responsible for the kHz QPOs. On the other hand, the time averaged spectra of LMXBs have been well studied by several missions. The primary component has been indisputably identified to be thermal Comptonization which typically dominates the spectrum especially at energies  $> 3$  keV. There is a secondary soft component which could be a multi-coloured disk emission (e.g. Mitsuda et al. 1984, 1989; Di Salvo et al. 2002; Agrawal and Misra 2009) or a black body from the boundary layer between the disk and the star (e.g. White et al. 1986; Di Salvo et al. 2001). The spectra show significant and systematic long term variation which is characterised by shapes (“Z” and “atoll”) in the colour-colour and colour-intensity plots. These variations are primarily due to the main thermal component. The temperature of the Comptonizing medium ranges from  $\sim 2$  keV (“soft” state) to  $\sim 15$  keV (“hard” state) while corresponding electron scattering optical depth ranges from  $\sim 10$  to  $\sim 2$  (e.g. Raichur, Misra, & Dewangan 2011).

The occurrence of kHz QPO has been reported to be related to the spectral shape or more specifically to the position of the source in its colour-colour diagram (Straaten, van der Klis, & Mendez 2003; Altamirano, et.al. 2008; Wijmands, et.al. 1997; Lin, et.al. 2012). The detection of the QPOs in the long term light curves of sources have also been examined (Yu, et.al. 1997; Mendez, et.al. 1998; Belloni, et.al. 2007). These studies seem to suggest that the QPOs are preferentially detected in intermediate spectral states which lie between the extreme soft and hard states. On the other hand, statistically analysis undertaken by Misra & Shanthi (2004) suggests that the fraction of segments having a kHz QPO is near unity at low states and decreases to zero at high states with nearly constant amplitude. In any case, irrespective of the details mentioned above, the kHz QPO is most probably associated with the primary thermal Comptonization component which typically dominates the spectra.

The fractional root mean square (r.m.s) amplitude of the kHz QPOs have been measured to be an increasing function of energy (Berger, et.al. 1996; Mendez, van der Klis, & Ford 2001; Zhang, et.al. 1996; Wijmands, et.al. 1997) with indications of a decrease at  $> 20$  keV (Mukherjee & Bhattacharyya 2012). This again implies that the phenomenon should be associated with the high energy thermal Comptonization component and not the soft black body one. Remarkable evidence was obtained when the time lag between different energy bins for the lower kHz QPO was measured to be of the order of  $\sim 30$  micro-seconds (Vaughan, et.al. 1997). For thermal Comptonization, higher energy photons scatter more than the low energy ones and hence one expects time-lags between them. For a corona of size of few kms and optical depths of order unity, the expected time difference is of the order of  $\sim 50$  micro-seconds. It was realised that the variation of the r.m.s and the time-lag as a function of energy is a powerful diagnostic which can distinguish which parameter (e.g. the plasma temperature, the soft photon input) drives the oscillation as well as constrain the size and geometry of the system (Lee, & Miller 1998). For the LMXB 4U 1608-52, the time lag was found to be “soft” i.e. the soft photons are delayed compared to the hard ones (erratum of Vaughan, et.al. 1997). Such soft lags were confirmed also for 4U 1636-53 (Kaaret, et.al. 1999). This is in apparent contradiction to the thermal Comptonization model, where one would expect hard lags. However, Lee, Misra, & Taam (2001) showed that if a fraction of the Comptonized photons impinge back in the soft photon source, then the system would show soft lags with an energy dependence similar to what has been observed.

Earlier, time lags for kHz QPOs were reported for a single RXTE observation of 4U 1608-52 (Vaughan, et.al. 1997) and 4U 1636-53 (Kaaret, et.al. 1999). Recently de Avellar, et.al. (2013) and Barret (2013) has analysed a number of observations of both sources and have confirmed that the time lag is soft and is of the order of tens of micro-secs for the lower kHz QPO. The time lag remains nearly constant till about  $\sim 800$  Hz and then decreases as the frequency increases. de Avellar, et.al. (2013) have studied for the first time the time-lag for the upper kHz QPO and find them to be hard lags and inconsistent with those seen for the lower kHz QPO. Thus, these results ascertain that time-lags in kHz QPOs is a rich phenomenon which can provide important insight into the nature of these systems.

Apart from delays due to electron scatterings in a thermal plasma, the time-lags could be due to other reasons. Longer time-lags ( $> 10$  msec) observed in the low frequency continuum (Nowak, et.al. 1999) are attributed to propagation of stochastic variability in a disk (Lyubarskii 1997; Misra 2000; Kotov, Churazov, & Gilfanov 2001) or for a low frequency QPO (e.g. Cui 1999), time-lag may be due to non-linear dependence of spectral parameters with each other (Misra & Mandal 2013). The micro-second time-lags observed for kHz QPOs are unlikely to be due to any of the above but could be due to reverberation of the X-rays from a reflector which is few kms away from the source (Barret 2013). However, it should be emphasised that since the primary spectral component is due thermal Comptonization, time lag due to multiple electron scattering must occur and should be of the order of tens of micro-seconds. Thus, while reverberation may contribute to the observed time-lags, the Comptonization lag is an important effect, which cannot be neglected for kHz QPOs.

In this work, we study using the linearised time dependent Kompaneets equation, the response of the thermal plasma to variations in the input photon flux and the plasma heating rate. For the latter, we also consider the possibility that a fraction of photons impinge back into the input photon source. The analysis predicts the shape of the r.m.s as a function of energy as well as the expected time-lags as a function of energy. We apply the method to a test case and show that such analysis can provide constraints on the geometry and size of the system.

In the next section we develop the mathematical formulation which is followed by §3 where the generic results are presented. In §4, as a test case, we apply the method to data from 4U 1608-52 to show the utility of such an analysis. In §5 we summarise and discuss the work.

## 2 VARIABILITY OF THERMAL COMPTONIZED PHOTONS

Thermal Comptonization is a process in which low energy “seed” photons are Comptonized by a hot thermal electron gas. While the geometry of the Comptonizing system in an X-ray binary may be complex, here we assume a simple one, where a spherical seed photon source of radius  $a$  is surrounded by a Comptonizing medium of width  $L$  and temperature  $T_e$ . The input source is considered to be a black body with temperature  $T_b$  and hence the rate of input photons per unit volume inside the medium is given as

$$\dot{n}_{s\gamma} = \left[ \frac{3a^2}{[(a+L)^3 - a^3]} \right] \left( \frac{2\pi}{h^3 c^2} \frac{E^2}{\left( \exp \left[ \frac{E}{kT_b} \right] - 1 \right)} \right) \quad (1)$$

The Thompson collision time scale is  $t_c = 1/(cn_e\sigma_T)$  and the optical depth of the medium is  $\tau = Ln_e\sigma_T$ , where  $\sigma_T$  is Thompson cross-section and  $n_e$  is the electron density. The evolution of the photon density,  $n_\gamma$ , inside the Comptonized medium in the non-relativistic limit (i.e.  $kT_e \ll m_e c^2$ ) and for low photon energies ( $E \ll m_e c^2$ ) is governed by the Kompaneets equation (Kompaneets 1957) where the

induced scattering term is neglected:

$$t_c \frac{dn_\gamma}{dt} = \frac{1}{m_e c^2} \frac{d}{dE} \left[ -4kT_e E n_\gamma + E^2 n_\gamma + kT_e \frac{d}{dE} (E^2 n_\gamma) \right] + t_c \dot{n}_{s\gamma} - t_c \dot{n}_{esc} \quad (2)$$

It should be noted that Eqn (2) describes the evolution of the photon density,  $n_\gamma$ , while typically the Kompaneets equation is often written in terms of the photon occupation number  $n \propto n_\gamma/E^2$ . In this work it is more intuitive to work directly with the photon density instead of the occupation number. Here  $\dot{n}_{esc}$  is the rate of escape of the photon density which is taken to be  $\dot{n}_{esc} \simeq \frac{n_\gamma}{(\tau^2 + \tau)t_c}$ . In steady state, the equilibrium photon density  $n_{\gamma o}$  can be computed by setting  $\frac{dn_\gamma}{dt} = 0$  and  $\dot{n}_{esc o}$  represents the emergent spectrum. The spectral shape is determined by the corresponding steady state values  $T_{eo}$ ,  $\tau_o$  and  $T_{bo}$ .

The electron temperature of the corona is set by the balance of Compton cooling and some external heating. In general the time evolution of the temperature is governed by

$$\frac{3}{2} k \frac{\partial T_e}{\partial t} = \dot{H}_{Ex} - \langle \Delta \dot{E} \rangle \quad (3)$$

where  $\dot{H}_{Ex}$  is the external heating rate per electron and the Compton cooling rate per electron is given by

$$\langle \Delta \dot{E} \rangle = \int_{E_{min}}^{E_{max}} (4kT_e - E) \frac{E}{m_e c^2} n_\gamma \sigma_T c dE \quad (4)$$

In steady state, when the electron temperature is  $T_{eo}$ ,  $\langle \Delta \dot{E} \rangle_o = \dot{H}_{Ex o}$ .

We take into account the possibility that a fraction,  $\eta$ , of the Comptonized photons impinge back onto to the seed photon source, thereby increasing the temperature of the seed photon source which can be estimated by

$$4\pi a^2 \sigma T_b'^4 = 4\pi a^2 \sigma T_b'^4 + \eta V_c \int \frac{n_\gamma}{(\tau^2 + \tau)t_c} E dE \quad (5)$$

where  $V_c = (4/3)\pi[(a+L)^3 - a^3]$  is the volume of the Comptonizing medium and  $T_b'$  is the input source temperature if  $\eta = 0$  i.e.  $4\pi a^2 \sigma (T_b')^4$  is the energy generation rate inside the seed photon source. If the variability amplitude of a source is small, then the time averaged spectrum will correspond to the steady state one with parameters,  $T_{eo}$ ,  $\tau_o$  and  $T_{bo}$ . For these values,  $T_{bo}'$  can be estimated to be

$$T_{bo}'^4 = T_{bo}^4 - \frac{\eta V_c}{4\pi a^2 \sigma} \int \frac{n_{\gamma o}}{(\tau^2 + \tau)t_c} E dE \quad (6)$$

and for the system there is a maximum allowed value of  $\eta$ ,  $\eta_{max}$  for which  $T_{bo}' = 0$ .

We consider small amplitude oscillation of the medium electron temperature and the source photon temperature over their average values i.e.  $T_e = T_{eo}(1 + \Delta T_e e^{-i\omega t})$ , and  $T_b = T_{bo}(1 + \Delta T_b e^{-i\omega t})$ . Here,  $\omega$  is the angular frequency of the oscillation and  $\Delta T_e \ll 1$  and  $\Delta T_b \ll 1$  are in general complex quantities. In the linear approximation, these will lead to variation in the photon density as  $n_\gamma = n_{\gamma o}(1 + \Delta n_\gamma e^{-i\omega t})$ . The oscillation amplitude of  $n_\gamma$ ,  $\Delta n_\gamma$  is related to  $\Delta T_e$  and  $\Delta T_b$  by the linearised Kompaneets equation, which is written in simplified form as (e.g. Lee, & Miller

1998; Lee, Misra, & Taam 2001)

$$\begin{aligned}
& -\frac{d^2 \Delta n_\gamma}{dE^2} + \left( \frac{-1}{kT_{eo}} - \frac{2}{n_{\gamma o}} \frac{dn_{\gamma o}}{dE} \right) \frac{d\Delta n_\gamma}{dE} \\
& + \frac{m_e c^2 t_c (\dot{n}_{s\gamma o} - i\omega n_{\gamma o})}{E^2 n_{\gamma o} kT_{eo}} \Delta n_\gamma = \left( \frac{-2}{E^2} + \frac{1}{n_{\gamma o}} \frac{d^2 n_{\gamma o}}{dE^2} \right) \Delta T_e \\
& + \frac{m_e c^2 t_c \dot{n}_{s\gamma o}}{E^2 n_{\gamma o} kT_{eo}} \left( \frac{\frac{E}{kT_{bo}}}{1 - \exp\left(\frac{-E}{kT_{bo}}\right)} \right) \Delta T_b \quad (7)
\end{aligned}$$

Here,  $\dot{n}_{s\gamma o}$  is the time averaged input photon rate. Solving Eqn 7 one gets the complex variation  $\Delta n_\gamma(E)$  as a function of energy, which can be used to compute the fractional r.m.s with energy,  $|\Delta n_\gamma(E)|$ , as well as phase lag between two energies  $E_1$  and  $E_2$  which is the argument of  $[\Delta n_\gamma(E_1) \Delta n_\gamma^*(E_2)]$ .

We consider two possible drivers of the variability of the system (i) variation in the seed photon temperature  $T_b$  and (ii) a variation in the external heating rate of the corona  $\dot{H}_{Ex}$  and analyse the induced temporal variation for both cases.

## 2.1 Variation of the seed photon temperature

A variation in the seed photon temperature i.e.  $T_b = T_{bo}(1 + \Delta T_b e^{-i\omega t})$  could be due to variation in the energy generation rate in the soft photon source. This will lead to a variation in the photon number density  $\Delta n_\gamma$  as governed by Eqn 7. The variation of the photon density would change the Compton cooling rate, leading to a variation in medium temperature,  $\Delta T_e$  which can be estimated by linearising Eqn (3) i.e.

$$\begin{aligned}
\frac{3}{2} kT_{eo} \Delta T_e(i\omega) &= \frac{\sigma_{TC}}{m_e c^2} \left[ \int 4kT_{eo}(\Delta T_e \right. \\
& \left. + \Delta n_\gamma) n_{\gamma o} E dE - \int E^2 \Delta n_\gamma n_{\gamma o} dE \right] \quad (8)
\end{aligned}$$

where we have assumed that the external heating rate of the corona is a constant at the steady state value,  $\dot{H}_{Ex} = \dot{H}_{Exo}$ .

The two complex differential equations (7) and (8) have to be solved simultaneously to obtain  $\Delta T_e$  and  $\Delta n_\gamma$  with the latter being a function of energy. We use an iterative numerical scheme to solve them. We start by having  $\Delta T_e = 0$  and obtain  $\Delta n_\gamma$  from Eqn (7). This is then used to get an updated value of  $\Delta T_e$  by Eqn (8). The procedure is iterated till  $\Delta T_e$  converges. For all computations done here, we find that the convergence is rapid and the converged value of  $\Delta T_e$  is obtained within a few iterations.

## 2.2 Variation of the coronal heating rate

A variation of the coronal heating i.e.  $\dot{H}_{Ex} = \dot{H}_{Exo}(1 + \Delta \dot{H}_{Ex} e^{-i\omega t})$ , would lead to a variation in the coronal temperature which is given by the linearised form of Eqn (3) i.e.

$$\begin{aligned}
\frac{3}{2} kT_{eo} \Delta T_e(-i\omega) &= \dot{H}_{Exo} \Delta \dot{H}_{Ex} - \frac{\sigma_{TC}}{m_e c^2} \left[ \int 4kT_{eo}(\Delta T_e \right. \\
& \left. + \Delta n_\gamma) n_{\gamma o} E dE - \int E^2 \Delta n_\gamma n_{\gamma o} dE \right] \quad (9)
\end{aligned}$$

The induced variation in the temperature would naturally lead to variations in the photon density. There is additional

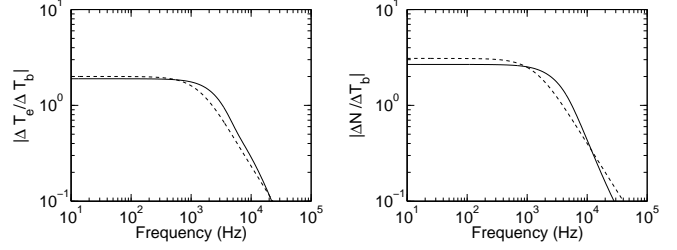


**Figure 1.** Variation of  $|\Delta T_e/\Delta T_b|$  and the energy integrated normalised photon density variation  $|\Delta N/\Delta T_b|$  as a function of frequency. Here  $\Delta N$  is the normalised integrated photon density variation in the energy band 2 - 60 keV i.e.  $\Delta N = \int n_\gamma \Delta n_\gamma dE / \int n_\gamma dE$ . The solid lines curves are for the “hard spectrum (Model A) and the dashed lines curves are for the “soft spectrum (Model B).

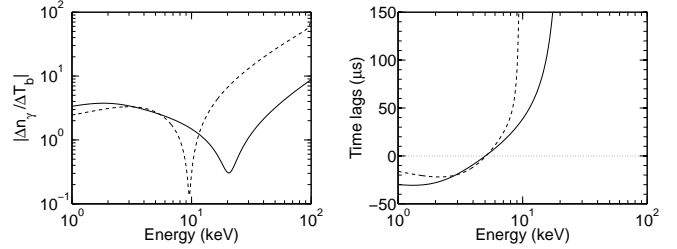


**Figure 2.** Variation of  $|\Delta n_\gamma/\Delta T_b|$  and time-lag as a function of photon energy. The solid lines curves are for the “hard spectrum (Model A) and the dashed lines curves marked B are for the “soft spectrum (Model B). The pivot point for both models is at high energies  $E \sim 10$ -20 keV and the time lags increase with energy which means that the hard photon lag the soft ones (i.e. hard lag).

complication because the photon density variation itself may lead to variations in the soft photon temperature, since a fraction of them are assumed to impinge back on to the soft photon source. This effect can be estimated by linearizing Eqn (5),

$$4\sigma(T_{bo})^4 \Delta T_b = \frac{\eta V_c}{4\pi a^2} \int \frac{n_{\gamma o}}{(\tau^2 + \tau)t_c} \Delta n_\gamma E dE \quad (10)$$

The three complex differential equations (7), (9) and (10) have to be solved simultaneously to obtain  $\Delta T_e$ ,  $\Delta T_b$  and  $\Delta n_\gamma$ . The solutions can be readily obtained in an iterative manner which converges rapidly.

## 3 RESULTS

To illustrate and to understand the energy dependent variability of the Comptonized photons, we consider two different steady state spectra. The first is a “hard” spectrum (Model A) characterised by relatively high temperature and low optical depth:  $kT_e = 15$  keV,  $\tau^2 = 6$  and a seed photon temperature of  $T_b = 0.3$  keV. The second is a “soft” spectrum (Model B) with low temperature and high optical depth,  $kT_e = 2.5$  keV,  $\tau^2 = 36$  and a seed photon temperature of  $T_b = 0.6$  keV. In practise, these time averaged values can be obtained by fitting the average spectrum with a steady state Comptonization model. Here we use these fiduciary parameter values to bring out qualitative differences between any hard and soft average spectra. For both

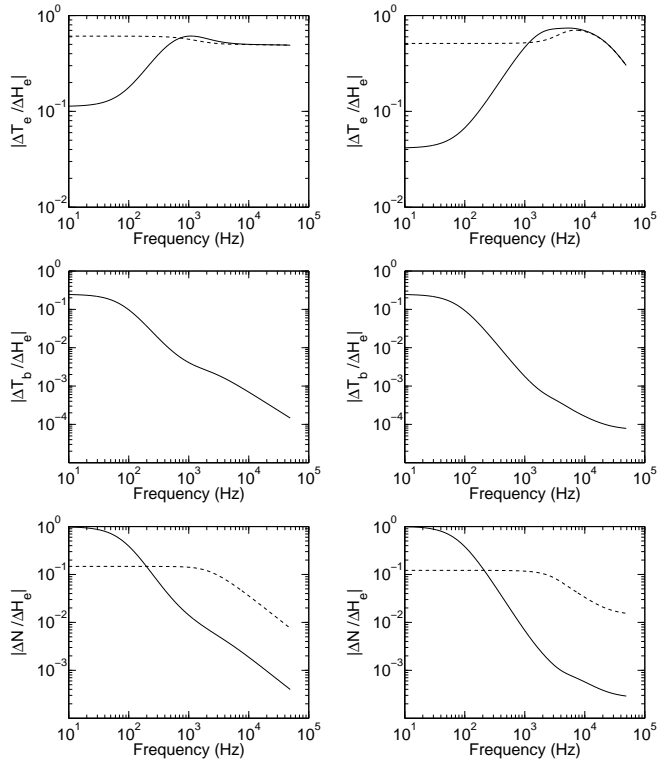


**Figure 3.** Variation of  $|\Delta T_e/\Delta H_e|$ ,  $|\Delta T_b/\Delta H_e|$  and the energy integrated normalised photon density variation  $|\Delta N/\Delta H_e|$  as a function of frequency. Here  $\Delta N$  is the normalised integrated photon density variation in the energy band 2 - 60 keV i.e.  $\Delta N = \int n_\gamma \Delta n_\gamma dE / \int n_\gamma dE$ . Left column is for the “soft spectrum (Model B) while the right column is for the “hard spectrum (Model A). The dotted lines are for  $\eta = 0$ , while the solid lines are for  $\eta = \eta_{max} = 0.59$  (soft spectrum) and  $0.28$  (hard spectrum).

models we choose the seed photon size  $a = 10$  km and the corona size to be  $L = 5$  km and the frequency of oscillation to be 850 Hz.

### 3.1 Variation of the seed photon temperature

Before studying the dependence with energy, we consider the behaviour of the system for different oscillation frequencies. The variation of the seed photon temperature leads to a variation of the corona temperature and the ratio  $|\Delta T_e/\Delta T_b|$  has been plotted in the top panel of Figure 1 for the “hard and “soft spectra. At low frequencies the coronal temperature responds to the seed photon variation with  $|\Delta T_e \sim 2\Delta T_b|$ , however at higher frequencies, the coronal temperature is unable to react to the rapid variation and hence varies significantly less. This is because at high frequencies the average photon density inside the corona fails to respond to rapid variation in the seed photons. This is illustrated in the right panel of Figure 1, where the energy integrated normalised photon density variation  $|\Delta N/\Delta T_b|$  is plotted as a function of frequency.  $\Delta N$  is the normalised integrated photon density variation in the energy band 2 - 60 keV, i.e.  $\Delta N = \int n_\gamma \Delta n_\gamma dE / \int n_\gamma dE$ . For both the “soft” and “hard” spectra, the photon density variation decreases sharply for frequencies larger than  $10^3$  Hz. The photon density variation in the corona will lead to variations in the escaping photons and hence  $|\Delta N|$  is proportional to the fractional

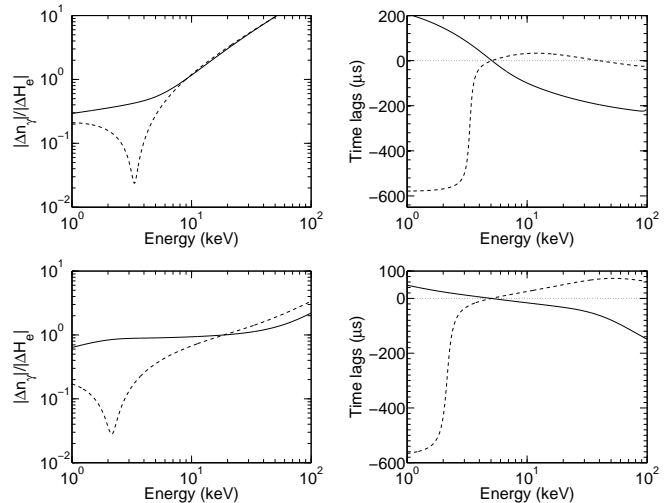


**Figure 4.** Variation of  $|\Delta n_\gamma|/|\Delta H_e|$  and time-lag as a function of photon energy. The top two figures are for the “soft spectrum (Model B) while the bottom two are for the “hard spectrum (Model A). The dotted lines are for  $\eta = 0$ , while the solid lines are for  $\eta = \eta_{max} = 0.59$  (soft spectrum) and  $0.28$  (hard spectrum). For  $\eta = 0$ , there is a pivot point at low energies  $E \sim 3$  keV, while for  $\eta = \eta_{max}$  there is no pivot point. For  $\eta = 0$  the time lags increase with energy (i.e. hard lag) while for  $\eta = \eta_{max}$  the trend reverses and the time lags decrease with energy (i.e. soft lag).

r.m.s observed from a source. Thus, for the system under consideration, fluctuations with r.m.s  $\sim 20\%$  is unlikely for frequencies  $> 10^4$  Hz, since that would imply large values of  $\Delta T_b \sim 1$ . For these curves, the size of the system is  $L = 5$  kms, and changing  $L$  will lead to a proportional horizontal shift in frequency. For  $L = 250$  kms  $|\Delta N/\Delta T_b| \sim 0.2$  for a frequency of  $\sim 10^3$  Hz. This implies that the observed kHz QPO, restricts the size to be less than  $L < 250$  kms, which is similar to the constrain obtained by light travel time arguments of  $L < c\delta T \sim 300$  kms.

The energy dependence of the photon density variation  $\Delta n_\gamma/\Delta T_b$  is shown in Figure 2 for the “hard” and “soft” spectra.  $\Delta n_\gamma$  is equal to the normalised r.m.s that can be obtained from observations. The frequency of oscillation is 850 Hz. There is a pivot point where the photon variation goes to zero and it is at high energies  $E \sim 10$ -20 keV. Below the pivot point, the variation is nearly constant or decreasing with energy. Also shown in Figure 2 is the expected lag between different energies. The time lag is an increasing function of energy while implies that the hard photon lag the soft ones (i.e. a hard lag).

### 3.2 Variation of the coronal heating rate

Variation of the coronal heating rate,  $\Delta H_e$  will induce a variation of the coronal temperature,  $\Delta T_e$  and their ratio as a function of frequency is plotted in Figure 3. If there is a fraction of photons which impinge back into the soft photon source (i.e.  $\eta \neq 0$ ), then there will be a variation of the seed photon temperature as well and this is plotted in the middle panel of Figure 3. The bottom panel shows the energy integrated photon density variation  $|\Delta N/\Delta H_e|$  as a function of frequency. For the Figure, we have considered

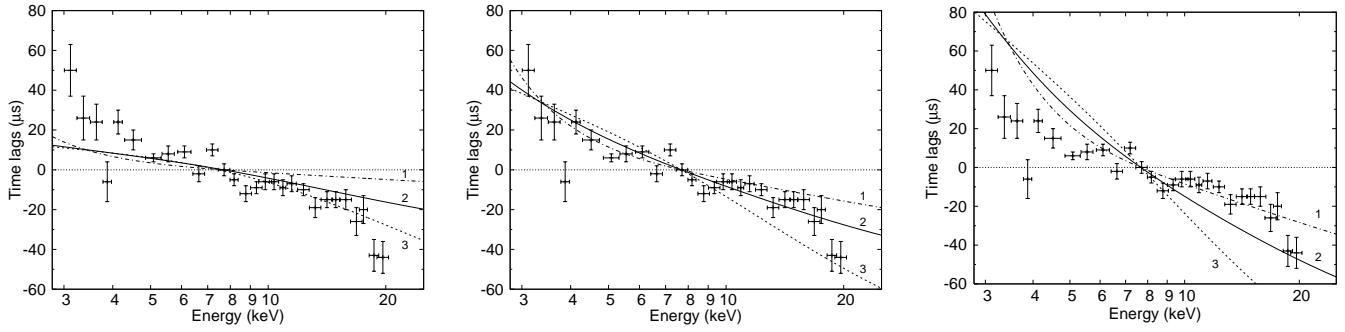


**Figure 5.** Time lags versus energy for the March 3rd observation of 4U 1608-52. The data is the same for all three panels. The left panel is for  $L = 0.3$  km and the curves marked 1, 2, and 3 are for  $\eta$  0.3, 0.5, and 0.57 respectively. The middle and right panels are for  $L = 1.0$  and 2.0 km and the curves marked 1, 2, and 3 are 0.3, 0.4, and 0.5 respectively. The best description of the data is obtained for  $L = 1$  km and  $\eta = 0.4$  (solid line in the middle panel).

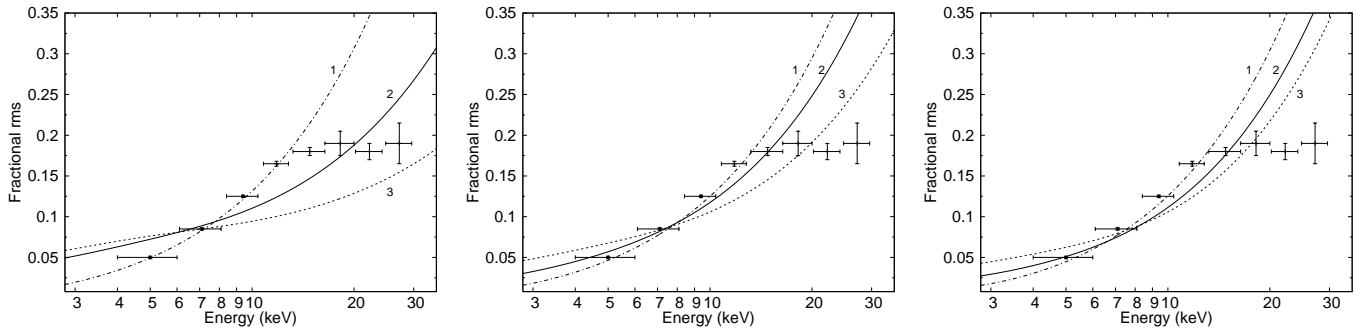


**Figure 6.** Fractional rms versus energy for the March 3rd observation of 4U 1608-52. The predicted lines correspond to the same parameters as used for the lines in Figure 5. Note that for energies  $< 20$  keV, the parameters that describe the lag variation ( $L = 1$  km and  $\eta = 0.4$ ) also describes the r.m.s versus energy (solid line in the middle panel).

two extreme cases of  $\eta = 0$  and  $\eta = \eta_{max}$ , where  $\eta_{max}$  is the maximum allowed fraction.

There is not much qualitative differences between the results of the “soft” and “hard” state spectra (left and right columns of Figure 3) which implies that the variability nature of such systems is not sensitive to the time averaged spectrum. However, there are important differences in the predicted variability of a system with  $\eta = 0$  and  $\eta = \eta_{max}$ . For  $\eta = 0$  the energy integrated photon variability,  $|\Delta N/\Delta H_e|$  is a constant and decreases for frequencies higher than  $10^3$  Hz, fairly similar to the results obtained for the case when the seed photon temperature is varied (Figure 1). For  $\eta = \eta_{max}$ ,  $|\Delta N/\Delta H_e|$  starts decreasing for frequencies  $> 100$  Hz and is  $\sim 0.05$  at  $\sim 1$  kHz. For any observed kHz QPO with fractional r.m.s  $> 5\%$ , would require an unphysically large variation in the heating rate  $|\Delta H_e| > 1$ . For such a system to be viable its size should be much smaller than  $L = 5$  kms assumed here. Note that this is a more stringent limit that that obtained from light travel time arguments of  $L < c\delta T \sim 300$  kms.

The variation of  $|\Delta n_\gamma/\Delta H_e|$  and time-lag as a function of photon energy are shown in Figure 4. Again, there are qualitative differences between the case when  $\eta = 0$  and  $\eta = \eta_{max}$ . For  $\eta = 0$ , the pivot point is at low energies while no pivoting is seen for  $\eta = \eta_{max}$ . More strikingly, the time lag behaviour changes. While for  $\eta = 0$ , the hard photons

lag the soft ones, the reverse occurs for  $\eta = \eta_{max}$ . Thus, in this interpretation soft lags occur only when a significant fraction of the Comptonized photons impinge back into the input photon source.

### 3.3 Comparison with the energy dependent time lags of 4U 1608-52

As discovered by Vaughan, et.al. (1997), the RXTE observation of the  $\sim 850$  Hz QPO of 4U 1608-52 on 3rd March 1996, remains one of the best cases of soft lag detection in kHz QPOs. Recently, Barret (2013) have estimated the time lag as a function of energy for more than 20 energy bins and have interpreted some of the qualitative features as due to reverberation lags. Thus, we choose this observation set as an example to illustrate how these time-lags can be interpreted in terms of Comptonization time delays and the possible constraints that can be obtained.

As shown in the previous section, soft time lags are expected only when the variation is in the coronal heating rate and with a significant fraction of photons impinging back into the input photon source. A detailed analysis can be undertaken only when the different components of the time-averaged spectrum are well constrained. In particular, the spectra of these sources require apart from a primary thermal component, a soft component modelled as a disk

black body and a broad Iron line, which implies the presence of a reflected component. The 3-10 keV low resolution spectrum obtained from the PCA observations are not sufficient to constrain these complex parameters. The absorption column density is undetermined and is often fixed to the Galactic value which might be an underestimate. Nevertheless, the primary component is the thermal Comptonization and when we fit a single thermal component model to the time averaged spectrum of this observation, we find that the model fits the data with a systematic uncertainty of 10%. The parameters obtained from such a fit, electron temperature  $kT_e = 2.6$  keV, optical depth  $\tau^2 = 40$  and soft photon temperature of 0.7 keV are similar to those obtained from more sophisticated analysis (e.g. Barret 2013). We defer a detailed analysis taking into account different spectral parameters to a latter work. Apart from the spectral parameters, there are two other important parameters which determine the time-lag versus energy. These are the size of the Comptonizing region,  $L$  and the fraction,  $\eta$  of photons impinging back into the input source. These two parameters can be constrained by comparison with the observed values.

The three panel in Figure 5 all show the observed time-lag versus energy for the observation which are compared with model predictions. The curves in the left, middle and right panels correspond to three different sizes of the Comptonizing regions,  $L = 0.3, 1.0$  and  $2.0$  kms respectively. The curves marked 1, 2, and 3 are for three different values of the fraction  $\eta$  mentioned in the caption. The best representation of the data occurs when  $L = 1.0$  km and  $\eta = 0.4$  (solid line in the middle panel). For smaller values of  $L = 0.3$  kms, the magnitude of the time-lag is smaller than observed, while for larger values,  $L = 2$  kms it is larger. Thus we demonstrate that time-lag analysis can well constrain the size of the Comptonizing region.

The model also predicts the r.m.s. versus energy for the QPO. In such a linear model, the normalisation of the r.m.s. scales with the magnitude of the perturbation  $\Delta T_e$ , but the shape of the curve is determined by the spectral parameters,  $\eta$  and the size  $L$  of the system. Figure 6 shows the variation of r.m.s versus energy for the same observation. The data points have been taken from Berger, et.al. (1996). The lines in the three panels are the predicted r.m.s for the model parameters used in Figure 5. It is interesting to note that for photon energies  $< 20$  keV, the predicted variation matches well with the observed values for  $L = 1$  km and  $\eta = 0.4$  (solid line of second panel in Figure 6). The observed r.m.s. is lower for higher energies possibly due to the presence of an additional constant hard component.

#### 4 SUMMARY AND DISCUSSION

The linearised time dependent Kompaneets equation describing thermal Comptonization has been solved self consistently taking into account energy balance of the plasma and soft photon source. When the perturbation is due to temperature variation in the soft photon source, the time-lag between photons of different energies is found to be hard. The fractional r.m.s as a function of energy reveals a pivot point at high energies and is nearly constant at lower energies. When the perturbation is in the heating rate of the plasma the pivot point is located at low energies. There is

a major qualitative change in the behaviour of the system if a significant fraction of the photons impinge back into the soft photon source. In this case, the time-lag is found to be soft and the r.m.s increases monotonically with energy. Such behaviour has been reported for the kHz oscillations in LMXBs. As an example, we compare the model predictions with the time-lag and r.m.s observed for the 850 Hz oscillation of 4U 1608-52 and show that the size of the Comptonizing region can be constrained to  $\sim 1$  km.

The analysis shows that modelling the time-lag and r.m.s variation as a function of energy for kHz QPOs is a powerful technique which can in principle constrain the size and geometry of the source. A more detailed analysis will require a careful modelling of the time-dependent spectra. Modelling the time-lag as well as the r.m.s at different QPO frequency and taking into account the corresponding spectral changes, may provide information regarding how the size and geometry of the system changes. Moreover, while the time-lags for the upper kHz QPO have not been constrained, they are known to be significantly different than those of the lower kHz QPO and hence should provide additional constraints. We defer such a detailed analysis to explain the observations reported by de Avellar, et.al. (2013) to a latter work. One may also need to take into account additional effects such as reverberation lags. The Iron line component and the soft disk emission may oscillate in response to the plasma variation after a time-lag. However, it is important to note that even for relatively small plasma size of  $\sim 1$ km, the time-lags due to Comptonization is of the order of  $\sim 50$  microseconds and hence they are expected to dominate. The more subtle and complicated General Relativistic effects may also be needed to be incorporated in order to correctly model such systems.

While the qualitative results such as the presence of soft lags do not depend on the time averaged spectral parameters, the constraints obtained on the size and geometry do depend on their precise values. Thus, it is important to obtain broad band spectral data during the time when a kHz QPO has been observed. This will be possible by the upcoming multi-wavelength satellite ASTROSAT<sup>1</sup> (Agrawal 2006) where the Large array X-ray proportional counter will detect the QPO while it and the other X-ray instruments will provide broad band spectra.

#### References

- Agrawal P. C., 2006, *Advances in Space Research*, 38, 2989
- Agrawal, V.K., Misra R., 2009, *MNRAS*, 398,1352
- Altamirano, D., van der Klis, M., Mendez, M., Jonker, P.G., Klein-Wolt, M., Lewin, W.H.G., 2008, *ApJ*, 685, 436
- Bachetti, M., Romanova, M.M., Kulkarni, A., Burderi, L., di Salvo, T., 2010, *MNRAS*, 403, 1193
- Barret, D., Olive, J.-F., Miller, M.C., 2005, *AN*, 326, 808
- Barret, D., 2013, *ApJ*, 770, 9
- Belloni, T., Mendez, M., Homan, J., 2005, *A&A*, 437, 209
- Belloni, T., Mendez, M., Homan, J., 2007, *MNRAS*, 376, 1133

<sup>1</sup> <http://astrosat.iucaa.in>

- Belloni, T., Homan, J., Motta, S., Ratti, E., Mandez, M., 2007, *MNRAS*, 379, 247
- Berger, M., van der Klis, M., van Paradijs, J., Lewin, W.H.G., Lamb, F., Vaughan, B., Kuulkers, E., Augusteijn, T., Zhang, W., Marshall, F.E., Swank, J.H., Lapidus, I., Lochner, J.C., Strohmayer, T.E., 1996, *ApJ*, 469, L13
- Cui W., 1999, *ApJ*, 524, L59
- de Avellar, M.G.B., Mendez, M., Sanna, A., Horvath, J.E., 2013, *MNRAS*, 433, 3453
- Di Salvo T. et al., 2001, *ApJ*, 554, 49
- Di Salvo T. et al., 2002, *A&A*, 386, 535
- Fragile, P.C., Mathews, G.J., Wilson, J.R., 2001 *ApJ*, 553, 955
- Kaaret, P., Piraino, S., Ford, E.C., Santangelo, A., 1999, *ApJ*, 514, L31
- Kato, S., 2007, *PASJ*, 59, 451
- Kato, S., 2009, *PASJ*, 61, 1237
- Kompaneets, A. S. 1957, *Soviet Phys. JETP*, 4, 730
- Kotov O., Churazov E., Gilfanov M., 2001, *MNRAS*, 327, 799
- Lamb, F.K., Miller, M.C., Psaltis, D., 1998, *Nuclear Physics B*, 69/1-3, 113
- Lamb, F.K., Miller, M.C., 2003, *astro-ph/0308179*, 10pp.
- Lee, H.C., Miller, G.S., 1998, *MNRAS*, 299, 479
- Lee, H.C., Misra, R., Taam, R.E., 2001, *ApJ*, 549, L229
- Li, X.-D., Zhang, C.-M., 2005, *ApJ*, 635, L57
- Lin, D., Remillard, R.A., Homan, J., Barret, D., 2012, *ApJ*, 756, 34
- Lin, Y.-G., Boutelier, M., Barret, D., Zhang, S.-N., 2011, *ApJ*, 726, 74
- Lovelace, R.V.E., Romanova M.M., 2007, *ApJ*, 670, L13
- Lovelace, R.V.E., Turner, L., Romanova M.M., 2009, *ApJ*, 701, 225
- Lyubarskii Y. E., 1997, *MNRAS*, 292, 679
- Mendez, M., van der Klis, M., Wijnands, R., Ford, E.C., van Paradijs, J., Vaughan, B.A., 1998, *ApJ*, 505, L23
- Mendez, M., van der Klis, M., Ford, E.C., 2001, *ApJ*, 561, 1016
- Mendez, M., 2006, *MNRAS*, 371, 1925
- Misra R., 2000, *ApJ*, 529, L95
- Misra R., Shanthi K., 2004, *MNRAS*, 354, 945
- Misra R., Mandal S., 2013, *ApJ*, 779, 71
- Mitsuda K., et al., 1984, *PASJ*, 36, 741
- Mitsuda K., Inoue H., Nakamura N., Tanaka Y., 1989, *PASJ*, 41, 97
- Miller, M.C., Lamb, F.K., Psaltis, D., 1998, *ApJ*, 508, 791
- Mukherjee A., Bhattacharyya S., 2012, *ApJ*, 756, 55
- Nowak, M.A., Vaughan, B.A., Wilms, J., Dove, J.B., Begelman, M.C., 1999, *ApJ*, 510, 874
- Osherovich, V., Titarchuk, L., 1999, *ApJ*, 522, L113
- Raichur H., Misra R., Dewangan G., 2011, *MNRAS*, 416, 637
- Remillard, R.A., and McClintock, J.E., 2006, *ARA&A*, 44, 49
- Sanna, A., Mendez, M., Belloni, T., Altamirano, D., 2012, *MNRAS*, 424, 2936
- Shi, C., Li, X.-D., 2009, *MNRAS*, 392, 264
- Stella, L., Vietri, M., 1999, *Phys. Rev. Lett.*, 82 17
- Straaten, S., van der Klis, M., Mendez, M., 2003, *ApJ*, 596, 1155
- Titarchuk, L., Osherovich, V., Kuznestov, S., 1999, *ApJ*, 525, L129
- Titarchuk, L., 2003, *ApJ*, 591, 354
- van der Klis, M. 2000, *ARA&A*, 38, 717
- van der Klis, M., 2006, *Compact Stellar X-ray Sources*, Chept. 2, eds. Lewin, W.H.G., and van der Klis, M. (Cambridge Astrophysics Series 39)
- Vaughan, B.A., van der Klis, M., Mendez, M., van Paradijs, J., Wijnands, R.A.D., Lewin, W.H.G., Lamb, F.K., Psaltis, D., Kuulkers, E., Oosterbroek, T., 1997, *ApJ*, 483, L115; erratum 509, L145 (1998)
- White N. E., et al., 1986, *MNRAS*, 218, 129
- Wijnands, R., Homan, J., van der Klis, M., Mendez, M., Kuulkers, E., van Paradijs, J., Lewin, W.H.G., Lamb, F.K., Psaltis, D., Vaughan, B., 1997, *ApJ*, 490, L157
- Yu, W., Zhang, S.N., Harmon, B.A., Paciesas, W.S., Robinson, C.R., Grindlay, J.E., Bloser, P., Barret, D., Ford, E.C., Tavani, M., Kaaret, P., 1997, *ApJ*, 490, L153
- Zhang, W., Lapidus, I., White, N.E., Titarchuk, L., 1996, *ApJ*, 469, L17
- Zhang, C., 2004, *A&A*, 423, 401